Robust Sahel drought due to the Interdecadal Pacific Oscillation in CMIP5 simulations.

Julián Villamayor[1] and Elsa Mohino[2]

Affiliation:

[1,2]Departamento de Física de la Tierra, Astronomía y Astrofísica I, Universidad Complutense de Madrid, Madrid, Spain.

Contact:

[1]Av. Complutense s/n, 28040 Madrid, Spain. julian.villamayor@fis.ucm.es

[2]Av. Complutense s/n, 28040 Madrid, Spain. emohino@fis.ucm.es

Abstract:

Many studies address the Interdecadal Pacific Oscillation (IPO) as a modulator of climate in several regions all over the globe. However very few suggest it has an impact on Sahel rainfall low-frequency variability. This work shows the relevance of such connection, supported by a robust response of state-of-the-art global climate models. Our results reveal that the positive phase of the IPO has a negative impact on Sahel rainfall anomalies regardless of the externally forced changes induced by anthropogenic gases. Such relationship is stronger for those models in which sea surface temperatures associated with the positive phase of the IPO show warmer anomalies over the Tropical Pacific. Therefore, we suggest the importance of a skillful simulation of IPO to improve decadal prediction of Sahel rainfall and to better understand its variability.

1. Introduction:

The Interdecadal Pacific Oscillation (IPO) is a low-frequency mode of variability usually defined as

the leading empirical orthogonal function (EOF) of the detrended sea surface temperature anomalies (SSTA) over the Pacific basin at decadal timescales (Figures 1a and 1b) [Zhang et al., 1997; Power et al., 1999]. The IPO is the basin-wide manifestation of the Pacific Decadal Oscillation (PDO), which is defined as the leading EOF of North Pacific detrended SSTA in winter [Mantua et al., 1997]. During its positive (negative) phase, the IPO sea surface temperature (SST) pattern is characterized by warm (cold) anomalies in the tropics and cold (warm) ones over the central and western extratropical Pacific (Figure 1b) [Trenberth and Hurrell, 1994; Meehl et al., 2009]. The origin of the mode is still under discussion. Some works suggest that it can arise by noise [Newman et al., 2003; Schneider and Cornuelle 2005; Shakun and Shaman, 2009], while others argue that the IPO is produced by atmosphere-ocean interactions involving the tropics and the extratropics [Deser et al., 2004; Meehl and Hu, 2006; Farneti et al., 2014]. Due to its vast temperature signal in the tropical Pacific, the IPO can offset or intensify the warming of globally averaged surface air temperatures [Gu and Adler, 2013; Meehl et al., 2013]. The IPO also impacts precipitation. It has been associated with drought conditions over the northern hemisphere summer monsoon [Hwang et al., 2013] and particularly over North America [Meehl and Hu, 2006; Dai, 2013] and in the Indian monsoon [Krishnan and Sugi, 2003; Meehl and Hu, 2006]; and has been shown to modulate the teleconnections of El Niño Southern Oscillation (ENSO) with rainfall over Australia [Power et al., 1999; Arblaster et al., 2002].

The Sahel is a semiarid region in West Africa extending between the humid savanna south of 10ºN and the beginning of the Sahara Desert at roughly 18ºN. The majority of the annual precipitation takes place in the boreal summer season, from July to September (JAS), and it is linked to the West African monsoon [Sultan and Janicot, 2003; Losada et al., 2010; Nicholson et al., 2013]. Due to the socio-economic importance of water resources in the region, the Sahel is highly vulnerable to rainfall variability. Throughout the 20th Century, Sahel precipitation has shown strong variability at decadal timescales [Mohino et al., 2011a]. Especially relevant was the prolonged period of drought

in the 1970s and 1980s, which draw the attention of many studies [e.g. Folland et al., 1986; Giannini et al., 2003; Dai et al., 2004; Caminade and Terray, 2010; Mohino et al., 2011a; Rodríguez-Fonseca et al., 2011]. There is currently a broad agreement that the main driver of Sahel precipitation at decadal timescales is SST variability amplified by land-surface processes [Zeng et al., 1999; Giannini et al., 2003; Kucharski et al., 2013].

Sahel rainfall variability is influenced by SST anomalies over different regions at multiple timescales. At interannual timescales, a warming of the equatorial Atlantic and ENSO-like SST anomalies over the Indo-Pacific promote drought over the Sahel [Janicot, 2001; Vizy and Cook, 2002; Giannini et al., 2005; Cook and Vizy, 2006; Joly and Voldoire, 2009; Mohino et al., 2011b; Losada et al., 2010, among others], while warmer conditions over the Mediterranean sea are linked to enhanced Sahel rainfall (Rowell, 2003). At decadal timescales, many works have highlighted the influence of the Atlantic Multidecadal Oscillation (AMO) on Sahel precipitation [e.g. Zhang and Delworth, 2006; Hoerling et al. 2006; Knight et al., 2006; Ting et al., 2009, 2011, 2014; Mohino et al., 2011a; Martin et al. 2014]. However, up to now, the few studies that have been done on the possible impact of the IPO on Sahel rainfall have shown a negative correlation (Figure 1c) [Joly, 2008; Mohino et al., 2011a] and a possible modulation of the effect of ENSO due to the IPO [Molion and Lucio, 2013].

In this study, we investigate the impact of the IPO on Sahel precipitation using the simulations from the Coupled Model Intercomparison Project – Phase V (CMIP5) [Taylor et al., 2012]. We particularly address the following questions: (1) Is there an impact of the IPO on Sahel precipitation? (2) What is the dynamical mechanism for such impact? (3) How do coupled models simulate the IPO and its impact over the Sahel? (4) Does the radiative forcing affect this relationship?

2. Data and Methods:

We work with monthly data of SST, precipitation and wind at high (200 hPa.) and low (850 hPa.) levels. To analyze the observed IPO and impacts we use HadISST1 [Rayner et al., 2003] and ERSSTv3 [Smith et al., 2008] SST reconstructions, CRUTS3.1 precipitation [Mitchel and Jones, 2005] and winds from the 20th Century Reanalysis [Compo et al., 2011]. For the simulations, the output from 17 different CMIP5 models is used, previously interpolated to a common regular grid with a spatial resolution of 2.8º in longitude and latitude. We have analyzed the unforced long-term preindustrial control (piControl) run; the historical run, which is a reproduction of the 20th century (typically from 1850-2005) with observed external forcing imposed; and the rcp8.5 future projection experiment, which considers the highest increase of anthropogenic gases concentration (see detailed list of models and simulations analyzed in Table S1 in the supplementary material).

Depending on the definition, some anthropogenic component can be included in the IPO index [Bonfils and Santer, 2011]. In order to isolate the internal variability of SSTs as much as possible, we remove the global component of the anthropogenic forcing in observations and forced simulations. To do so, we calculate a “residual” field from the annual mean SSTA following Mohino et al. [2011a]: We define a global warming (GW) index as the lowpass-filtered (40-yr cutoff) time series of averaged SSTA between 45ºS and 60ºN. We regress the original SSTA onto the GW index and we construct a “GW fitted” SSTA field by multiplying the regression coefficient at each grid point by the GW index. Finally, we subtract the “GW fitted” SSTA field from the original one and obtain the “residual" SSTA field. To focus on decadal timescales, the “residual” field is lowpass-filtered (13-yr cutoff).

The IPO indices from observations and the forced simulations (historical and rcp8.5 experiments) are then defined as the first principal component (PC) of the “residual” SSTA, associated to the first

Empirical Orthogonal Function (EOF) calculated over the Pacific basin (between 60ºN-45ºS). The members of the residual SSTA of the models with several realizations available are concatenated in time before applying the EOF analysis. For the externally unforced piControl simulations the IPO index is defined as the PC associated with the first EOF of the 13-year lowpass-filtered original SSTA field.

Once the IPO index of each model is calculated, the model SST and rainfall patterns are obtained by regressing the unfiltered fields onto the IPO index. To highlight the consistent response from models, the patterns from the 17 models are averaged together. The statistical significance of the averaged patterns is evaluated with a Monte Carlo-based test (see details in supplementary material).

3. Results:

In accordance with previous studies [Mantua et al., 1997; Mantua and Hare, 2002; Deser et al., 2004; Shen et al., 2006; Mohino et al., 2011a; Dai, 2013], the observed IPO index shows cold regimes in the periods of 1909-1925, 1944-1976 and from 1998 onwards, and warm regimes in the periods 1925-1944 and 1976-1998 (Figure 1a). However, such time variability shows no dominant frequency but various spectral peaks at decadal and multidecadal periodicities, mainly in the 15-25 and 50-70 year bands (Figure S1), in accordance with previous works [Minobe, 1999; Chao et al., 2000; Tourre at al., 2001; Mantua and Hare, 2002; MacDonald and Case, 2005]. On average, models tend to show higher power spectra in two frequency bands, one close to 50-70 years and the other one close to 15-25 years (Figure S2). This suggests that, though there is no clear well-defined periodicity for the IPO (in accordance with the proxy reconstruction from Shen et al. [2006]), the power spectra in models and observations tends to cluster around two preferred bands, of approximately 15-25 and 50-70 years.

The SST pattern associated with the IPO in the historical and control simulations is consistent with observations (Figures 2a, 2c and 1b): In the Pacific, there are cold anomalies over the western part of the basin, poleward of 25º and more prominent in the Northern Hemisphere. There are also warm anomalies over the Tropical Pacific, and over the north and south of the eastern part of the basin. Outside the Pacific basin, the models show a less consistent response among themselves and with the observations. There are, however, regions of anomalous warming over the Indian Ocean, the Tropical Atlantic and next to the southeast coast of Brazil in both simulations and in the observations. The agreement among models on the SST pattern associated with the IPO is weaker in the historical runs than in the piControl ones.

Associated with a positive IPO, the models simulate a significant pattern of negative precipitation anomalies across the Sahel (Figures 2b and 2d), in accordance with observations (Figure 1c). Nevertheless, the observed positive anomalies of precipitation on the coastal area of Guinea, Sierra Leone and Liberia are not reproduced in the simulations. Models underestimate the intensity of the precipitation anomalies in comparison to observations (note different scales on Figure 1c and Figures 2b and 2d). Apart from the attenuation produced by the model mean, the individual models also show this underestimation (Figures S5 and S6). Such underestimation of Sahel rainfall is consistent with an underestimated atmospheric response over West Africa at low and middle levels (not shown). We speculate that the origin of the underestimation could be attributed to the weak rainfall response that Atmospheric General Circulation Models forced with prescribed SSTs show over the Sahel at these time scales [e.g. Rodríguez-Fonseca et al., 2011; Joly et al. 2007; Kucharski et al., 2013], and could be related to the accuracy with which the vegetation-atmosphere feedbacks are parameterized [Giannini et al., 2003; Wang et al., 2007]. It should be noted that, despite the high resemblance between the precipitation patterns coming from both experiments, the agreement among models is higher in the piControl run than in the historical one.

Sahel drought in response to the IPO is a remarkably consistent feature across models and simulations (Figure 3a). For both, historical and piControl experiments, 13 out of the 17 models analyzed simulate a negative correlation between the IPO and the unfiltered Sahel precipitation index. The larger correlation coefficients obtained for the observations suggest a stronger relationship in the real world. The scatter plot in Figure 3b shows that the stronger the SSTA warming over the tropical Pacific, the stronger the IPO's impact on Sahel drought. There are, however, a few models (4 out of 17 models in each experiment) that produce a positive impact of the IPO on Sahel rainfall, though most of these impacts are not statistically significant. These models tend to show a poorly defined IPO spatial pattern in the Pacific basin with weak positive or even negative SSTA over the Tropical Pacific (inmcm4 and MRI-CGCM3 for the historical simulation and GISS-E2-H and GISS-E2-R for the piControl one; Figures S3 and S4). However, some models with a weak or even positive Sahel rainfall response to IPO show warm SSTA over the Tropical Pacific (for instance the CSIRO-Mk3-6-0 model in both experiments; Figures S3 and S4). The positive SSTA over the northeastern Tropical Atlantic basin, with comparable magnitude to the ones over the Pacific warm tongue could partly explain this behaviour (Figures S3 and S4). Such northeastern Tropical Atlantic SSTA has been shown to promote increased rainfall over Sahel [Cook and Vizy, 2006; Giannini et al., 2013] and could be overriding the Tropical Pacific influence in some cases. When both regions, Tropical Pacific and northeastern Tropical Atlantic (boxed areas in Figures 2a), are used to calculate the scatter plot (Figure S7), the explained inter-model variance increases from 0.26 to 0.33, which suggests that a strong negative Sahel precipitation response to IPO is linked to a strong warming over the Tropical Pacific and weak anomalies over the Tropical North Atlantic (Figure 3b).

In observations and simulations, a positive IPO is associated with anomalous convergence over the central Tropical Pacific and divergence over the Tropical Atlantic and West Africa at low levels, and

with anomalous divergence and convergence over these two regions, respectively, at high levels (Figure 4). This suggests an anomalous Walker-type overturning cell that connects upward movements over the central Pacific in response to local warm SSTAs there with subsidence over West Africa. This, in turn, reduces the Tropical Easterly Jet and the low-level monsoon westerlies, weakening the monsoon (not shown) and leading to drought conditions over the Sahel. Such mechanism was also proposed for the impact of ENSO events on Sahel rainfall [Janicot, 2001; Joly and Voldoire, 2009; Mohino et al., 2011b]. The similarity between the teleconnection mechanisms at different time scales is consistent with the similar SST patterns over the Tropical Pacific observed for the ENSO and IPO [Deser et al., 2004].

4. Discussion:

The similarity between the SSTA patterns of the historical and the unforced piControl simulations suggests that the IPO SST mode is mainly produced by the internal variability of the models, and that radiative effects do not play a relevant role. However, it is also noticeable that the patterns associated with the IPO are more consistent among models in the piControl experiments than in the historical ones (Figure 2). The methodology we use to obtain the residual SSTA in observations and in the forced runs eliminates the long-term global component of the external forcing. However the external component with more localized effects is not removed. This is especially relevant in the case of aerosols, for which important uncertainties still remain [Boucher et al., 2013]. Such uncertainties could translate into a slightly different behavior of the residual SSTA among models in some regions and, thus, to a less robust SSTA pattern response to IPO in historical simulations than in piControl ones.

Since the models are able to reproduce a modulation of Sahel rainfall by the IPO robustly and congruent to what was observed over the last century, we consider if this relationship will change in

the future. The majority of models project an increase of Sahel rainfall for mid- and late 21st century under rcp8.5 scenario, though the presence of outliers and the increase of the inter-model dispersion with time suggest a high degree of uncertainty [Biasutti, 2013; Vizy et al., 2013]. The SSTA IPO pattern for the rcp8.5 simulations is similar to the historical and piControl simulations (Figure 5a). This suggests that under conditions of high anthropogenic gases concentrations, the Pacific internal processes that generate the IPO SST pattern will not be altered. However, the consistency among models is lower than in the other experiments. Difficulties to capture IPO-like SSTA patterns of some models with respect to the other simulations (i.e. bcc-csm1-1, CNRM-CM5, HadGEM2-ES and NorESM1-M) introduce more discrepancies across all models (Figure S9). As in the historical pattern, this may be due to the methodology used to extract the external forcing. Note that the rcp8.5 future projection introduces a stronger radiative forcing and may induce more discrepancies between models when computing the residual SSTA. In addition, the rcp8.5 runs are shorter (typically from 2006-2100, detailed in Table S1) and the IPO-like decadal variability may not be properly captured with an EOF analysis. The impact of the rcp8.5 IPO on rainfall (Figure 5b) is also negative on the Sahel as in the other simulations and it is produced by a similar atmospheric mechanism (Figure S8). Therefore the CMIP5 simulations suggest that the SSTA pattern associated with the IPO variability mode is not expected to change in the future nor its impact on Sahel precipitation.

We must highlight the strong consistency across CMIP5 models found in this work in reproducing the observed IPO modulation of Sahel rainfall low-frequency variability. Conversely, the AMO relationship with Sahel rainfall, which has been broadly studied [e.g. Zhang and Delworth, 2006; Hoerling et al., 2006; Knight et al., 2006; Ting et al., 2009, 2011, 2014; Mohino et al., 2011a], is not as consistently reproduced by CMIP5 models [Martin et al., 2014]. Therefore, although the influence of the AMO is greater than that of the IPO in observations, our results suggest that climate models might not behave in the same way when analyzing the decadal variability of the Sahel

rainfall led by modes of SST variability.

5. Summary and conclusions:

In this work we show that most CMIP5 global climate models reproduce a consistent and well-defined IPO SST pattern with a robust negative (positive) impact on Sahel rainfall linked to its positive (negative) phase. This result coincides with observations and supports the hypothesis that the IPO modulates decadal variability of Sahel rainfall through an anomalous Walker-type circulation that produces subsidence over West Africa in the positive phase. The skill of each model to simulate this connection is related to the IPO SSTA pattern. Models reproducing a well-defined Tropical Pacific warm tongue have a significant negative IPO impact on Sahel rainfall, while models with weak Tropical Pacific SSTAs compared to the northeastern Tropical Atlantic ones show a small impact over the Sahel.

The small differences between the IPO SSTA and Sahel rainfall patterns from forced and unforced simulations suggest that the IPO is mainly an internal mode. From our analysis of rcp8.5 future projections we expect that the IPO SST mode and its influence on Sahel rainfall will not change in the future even if there is an increase of anthropogenic gases concentration.

Skill in decadal predictions of Sahel rainfall are model dependent and have been mainly attributed to the skillful reproduction of AMO related SSTs [van Oldenborgh et al., 2012; García-Serrano et al., 2013; Gaetani and Mohino, 2013]. Current GCMs show very low skill in predicting the SST anomalies associated with the IPO [Kim et al., 2012; Doblas-Reyes et al., 2013; Kirtman et al., 2013] and Newman [2013] showed that similar or even better skill could be obtained with a linear inverse model. Our results suggest that an improved characterization of the predicted SSTA pattern and timing of IPO events could be key to enhancing the skill of Sahel rainfall decadal predictions.

6. Acknowledgements:

The authors thank the helpful comments of the two anonymous reviewers and the editor Dr. Diffenbaugh. The research leading to these results has received funding from the European Union Seventh Framework Programme (FP7/2007-2013) under grant agreement n° 603521 and the Spanish project CGL2012-38923-C02-01. We acknowledge the World Climate Research Programme's Working Group on Coupled Modelling, which is responsible for CMIP, and we thank the climate modelling groups for producing and making available their model output. For CMIP the U.S. Department of Energy's Program for Climate Model Diagnosis and Intercomparison provides coordinating support and led development of software infrastructure in partnership with the Global Organization for Earth System Science Portals. Thanks are also given to the MICINN of the Spanish Government for the Scholarship that JV has been granted.

7. References:

Arblaster, J., G. Meehl, and A. Moore (2002), Interdecadal modulation of Australian rainfall, *Clim. Dyn*., 18(6), 519–531.

Biasutti, M. (2013), Forced Sahel rainfall trends in the CMIP5 archive, *J. Geophys. Res. Atmos.*, 118, 1613–1623, doi:10.1002/jgrd.50206.

Bonfils, C., and B. D. Santer (2011), Investigating the possibility of a human component in various pacific decadal oscillation indices, *Clim. Dyn.*, 37(7–8), 1457–1468.

286 Boucher, O., D. Randall, P. Artaxo, C. Bretherton, G. Feingold, P. Forster, V. -M. Kerminen, Y.
287 Kondo, H. Liao, U. Lohmann, P. Rasch, S. K. Satheesh, S. Sherwood, B. Stevens and X. Y. Zhang
288 (2013), Clouds and Aerosols, in Climate Change 2013: The Physical Science Basis, Contribution of
289 Working Group I to the Fifth Assessment Report of the Intergovernmental Panel on Climate Change
290 [Stocker, T.F., D. Qin, G.-K. Plattner, M. Tignor, S.K. Allen, J. Boschung, A. Nauels, Y. Xia, V. Bex
291 and P.M. Midgley (eds.)] , pp 571–657, Cambridge University Press, Cambridge, United Kingdom
292 and New York, NY, USA.
293
294 Caminade, C., and L. Terray (2010), Twentieth century Sahel rainfall variability as simulated by the
295 ARPEGE AGCM, and future changes, *Clim. Dyn.*, 35, 75–94.
296
297 Chao, Y., M. Ghil, and J. C. McWilliams (2000), Pacific interdecadal variability in this century's sea
298 surface temperatures, *Geophys. Res. Lett*., 27(15), 2261–2264.
299
300 Compo, G. P., J. S. Whitaker, P. D. Sardeshmukh, N. Matsui, R. J. Allan, X. Yin, B. E. Gleason, R.
301 S. Vose, G. Rutledge, P. Bessemoulin, S. Brönnimann, M. Brunet, R. I. Crouthamel, A. N. Grant, P.
302 Y. Groisman, P. D. Jones, M. C. Kruk, A. C. Kruger, G. J. Marshall, M. Maugeri, H. Y. Mok, Ø.
303 Nordli, T. F. Ross, R. M. Trigo, X. L. Wang, S. D. Woodruff, and S. J. Worley (2011), The
304 Twentieth Century Reanalysis Project, *Q.J.R. Meteorol. Soc*., *137*, 1–28, doi: 10.1002/qj.776.
305
306 Cook, K. H., and E. K. Vizy (2006), Coupled Model Simulations of the West African Monsoon
307 System: Twentieth- and Twenty-First-Century Simulations, *J. Clim.*, 19(15), 3681–3703.
308
309 Dai, A., P. J. Lamb, K. E. Trenberth, M. Hulme, P. D. Jones, and P. Xie (2004), The recent Sahel
310 drought is real, *Int. J. Climatol*., 24, 1323–1331.
311

312 Dai, A. (2013), The influence of the inter-decadal Pacific oscillation on US precipitation during
313 1923–2010, *Clim. Dyn*., 41(3–4), 633–646.
314
315 Deser, C., A. S. Phillips, and J. W. Hurrell (2004), Pacific Interdecadal Climate Variability:
316 Linkages between the Tropics and the North Pacific during Boreal Winter since 1900, Journal of
317 Climate, 17(16), 3109–3124.
318
319 Doblas-Reyes, F. J., I. Andreu-Burillo, Y. Chikamoto, J. García-Serrano, V. Guemas, M. Kimoto, T.
320 Mochizuki, L. R. L. Rodrigues, and G. J. van Oldenborgh (2013), Initialized near-term regional
321 climate change prediction, *Nature Comms.*, 4, 1715, doi:10.1038/ncomms2704.
322
323 Farneti, R., F. Molteni, and F. Kucharski (2014), Pacific interdecadal variability driven by
324 tropical-extratropical interactions, *Clim. Dyn*., 42, 11–12, 3337–3355.
325
326 Folland, C. K., T. N. Palmer, D. E. Parker (1986), Sahel rainfall and worldwide sea temperatures,
327 1901-85, *Nature*, 320, 602–607, doi:10.1038/320602a0.
328
329 Gaetani, M., and E. Mohino (2013), Decadal prediction of the Sahelian precipitation in CMIP5
330 simulations, *J. Clim*., 26, 7708–7719. doi:10.1175/JCLI-D-12-00635.1.
331
332 García-Serrano, J., F. J. Doblas-Reyes, R. J. Haarsma, and I. Polo (2013), Decadal prediction of the
333 dominant West African monsoon rainfall modes, *J. Geophys. Res.*, 118, 5260–5279.
334
335 Giannini, A., R. Saravannan, and P. Chang (2003), Oceanic forcing of Sahel rainfall on interannual
336 to interdecadal time scales, *Science*, 302, 1027–1030.
337

338 Giannini A, R. Saravannan, P. Chang (2005), Dynamics of the boreal summer African monsoon in
339 the NSIPP1 atmospheric model, *Clim.Dyn.*, 25:517–535, doi:10.1007/s00382-005–0056.
340
341 Giannini, A., S. Salack, T. Lodoun, A. Ali, A. T. Gaye, and O. Ndiaye (2013), A unifying view of
342 climate change in the Sahel linking intra-seasonal, interannual and longer time scales, *Environ. Res.*
343 *Lett.*, 8, 024010, doi:10.1088/1748-9326/8/2/024010.
344
345 Gu, G., and R. F. Adler (2013), Interdecadal variability/long-term changes in global precipitation
346 patterns during the past three decades: global warming and/or pacific decadal variability?, *Clim.*
347 *Dyn.*, 40(11–12), 3009–3022.
348
349 Hoerling, M., J. Hurrell, J. Eischeid, and A. Phillips (2006), Detection and attribution of twentieth-
350 century northern and southern African rainfall change, *J. Clim.*, 19(16), 3989–4008.
351
352 Hwang, Y. T., D. M. Frierson, and S. M. Kang (2013), Anthropogenic sulfate aerosol and the
353 southward shift of tropical precipitation in the late 20th century, *Geophys. Res. Lett.*, 40(11), 2845–
354 2850.
355
356 Janicot, S., S. Trzaska, and I. Poccard (2001), Summer Sahel-ENSO teleconnection and decadal
357 time scale SST variations, *Clim. Dyn.*, 18(3–4), 303–320.
358
359 Joly, M. (2008), Rôle des océans dans la variabilité climatique de la Mousson Africaine, Ph.D.
360 thesis, Univ. of Paris-Est, Paris, France.
361

362 Joly, M., A. Voldoire, H. Douville, P. Terray, and J. F. Royer (2007), African monsoon
363 teleconnections with tropical SSTs: validation and evolution in a set of IPCC4 simulations, *Clim.*
364 *Dyn*., 29(1), 1–20.
365
366 Joly, M., and A. Voldoire (2009), Influence of ENSO on the West African monsoon: temporal
367 aspects and atmospheric processes, *J. Clim.*, 22(12), 3193–3210.
368
369 Kim, H. M., P. J. Webster, and J. A. Curry (2012), Evaluation of short-term climate change
370 prediction in multi-model CMIP5 decadal hindcasts, *Geophys. Res. Lett.*,
371 doi:10.1029/2012GL051644.
372
373 Kirtman, B., S. B. Power, J. A. Adedoyin, G. J. Boer, R. Bojariu, I. Camilloni, F. J. Doblas-Reyes,
374 A. M. Fiore, M. Kimoto, G. A. Meehl, M. Prather, A. Sarr, C. Schär, R. Sutton, G. J. van
375 Oldenborgh, G. Vecchi and H. J. Wang (2013), Near-term Climate Change: Projections and
376 Predictability, in Climate Change 2013: The Physical Science Basis, Contribution of Working
377 Group I to the Fifth Assessment Report of the Intergovernmental Panel on Climate Change
378 [Stocker, T.F., D. Qin, G.-K. Plattner, M. Tignor, S.K. Allen, J. Boschung, A. Nauels, Y. Xia, V. Bex
379 and P.M. Midgley (eds.)], pp 953–1028, Cambridge University Press, Cambridge, United Kingdom
380 and New York, NY, USA.
381
382 Knight, J. R., C. K. Folland, and A. A. Scaife (2006), Climate impacts of the Atlantic Multidecadal
383 Oscillation, *Geophys. Res. Lett.*, 33, doi:10.1029/2006GL026242.
384
385 Krishnan, R., and M. Sugi (2003), Pacific decadal oscillation and variability of the Indian summer
386 monsoon rainfall, *Clim. Dyn.*, 21(3–4), 233–242.
387

388 Kucharski, F., F. Molteni, M. P. King, R. Farneti, I. S. Kang, and L. Feudale (2013), On the need of
389 intermediate complexity general circulation models: a ”SPEEDY” example, *Bull. Amer. Meteor.*
390 *Soc.*, 94, 25–30, doi: 10.1175/BAMS-D-11-00238.1.
391
392 Losada, T., B. Rodríguez-Fonseca, S. Janicot, S. Gervois, F. Chauvin, and P. Ruti (2010), A multi-
393 model approach to the Atlantic Equatorial mode: impact on the West African monsoon, *Clim. Dyn.*,
394 35, 29–43, doi:10.1007/s00382-009-0625-5.
395
396 MacDonald, G. M., and R. A. Case (2005), Variations in the Pacific Decadal Oscillation over the
397 past millennium, *Geophys. Res. Lett.*, 32(8).
398
399 Mantua, N. J., S. R. Hare, Y. Zhang, J. M. Wallace, and R. C. Francis (1997), A Pacific interdecadal
400 climate oscillation with impacts on salmon production, *Bull. Am. Meteorol. Soc.*, 78, 1069–1079.
401
402 Mantua, N. J., and S. R. Hare (2002), The Pacific Decadal Oscillation, *J. Oceanogr.*, 58, 35–44.
403
404 Martin, E. R., C. Thorncroft, and B. B. B. Booth (2014), The Multidecadal Atlantic SST-Sahel
405 Rainfall Teleconnection in CMIP5 Simulations, *J. Clim.*, *27*, 784–806, doi:10.1175/JCLI-D-13-
406 00242.1.
407
408 Meehl, G. A., and A. Hu (2006), Megadroughts in the Indian monsoon region and southwest North
409 America and a mechanism for associated multidecadal Pacific sea surface temperature anomalies, *J.*
410 *Clim.*, 19(9), 1605–1623.
411
412 Meehl, G. A., A. Hu, and B. D. Santer (2009), The mid-1970s climate shift in the Pacific and the
413 relative roles of forced versus inherent decadal variability, *J. Clim.*, 22, 780–792.

Meehl, G. A., A. Hu, J. M. Arblaster, J. Fasullo, and K. E. Trenberth (2013), Externally forced and internally generated decadal climate variability associated with the Interdecadal Pacific Oscillation, *J. Clim.*, 26(18), 7298–7310.

Minobe, S. (1999), Resonance in bidecadal and pentadecadal climate oscillations over the North Pacific: Role in climatic regime shifts, *Geophys. Res. Lett*., 26, 855–858.

Mitchel, T. D., and P. D. Jones (2005), An improved method of constructing a database of monthly climate observations and associated high-resolution grids, *Int. J. Climatol*., *25*, 693–712, doi:10.1002/joc.1181.

Mohino, E., S. Janicot, and J. Bader (2011a), Sahel rainfall and decadal and multi-decadal sea surface temperature variability, *Clim. Dyn.*, 37, 419–440, doi:10.1007/s00382-010-0867-2.

Mohino, E., B. Rodríguez-Fonseca, C. R. Mechoso, S. Gervois, P. Ruti and F. Chauvin (2011b), Impacts of the Tropical Pacific/Indian Oceans on the Seasonal Cycle of the West African Monsoon, *J. Clim.*, 24, 3878–3891 doi:10.1175/2011JCLI3988.1.

Molion, L. C. B., and P. S. Lucio (2013), A Note on Pacific Decadal Oscillation, El Nino Southern Oscillation, Atlantic Multidecadal Oscillation and the Intertropical Front in Sahel, Africa, *Atmos. Clim. Sci.*, 3, doi:10.4236/acs.2013.33028.

Newman, M., G. P. Compo, and M. A. Alexander (2003), ENSO-forced variability of the Pacific decadal oscillation, *J. Clim.*, 16(23), 3853–3857.

Newman, M. (2013), An empirical benchmark for decadal forecasts of global surface temperature anomalies, *J. Clim.*, 26(14), 5260–5269.

Nicholson, S. E. (2013), The West African Sahel: A review of recent studies on the rainfall regime and its interannual variability, *ISRN Meteorol,* 2013, 453521.

van Oldenborgh, G. J., F. J. Doblas-Reyes, B. Wouters, and W. Hazeleger (2012), Decadal prediction skill in a multi-model ensemble, *Clim. Dyn.*, 38, 1263–1280.

Power, S., T. Casey, C. Folland, A. Colman, and V. Mehta (1999), Inter-decadal modulation of the impact of ENSO on Australia, *Clim. Dyn.*, 15, 319–324.

Rayner, N. A., D. E. Parker, E. B. Horton, C. K. Folland, L. V. Alexander, and D. P. Rowell (2003), Global analyses of sea surface temperature, sea ice, and night marine air temperature since the nineteenth century, *J. Geophys. Res.*, *108*. doi:10.1029/2002JD002670.

Rodríguez-Fonseca, B., S. Janicot, E. Mohino, T. Losada, J. Bader, C. Caminade, F. Chauvin, B. Fontaine, J. García-Serrano, S. Gervois, M. Joly, I. Polo, P. Ruti, P. Roucou, and A. Voldoire (2011), Interannual and decadal SST forced responses of the West African monsoon, *Atmos. Sci. Lett*., 12, 67–74, doi: 10.1002/ASL.308.

Schneider, N., and B. D. Cornuelle (2005), The Forcing of the Pacific Decadal Oscillation*, *J. Clim.*, 18(21), 4355–4373.

Shakun, J. D., and J. Shaman (2009), Tropical origins of North and South Pacific decadal variability, *Geophys. Res. Lett.*, 36(19), doi:10.1029/2009GL040313.

Shen, C., W. C. Wang, W. Gong, and Z. Hao (2006), A Pacific Decadal Oscillation record since 1470 AD reconstructed from proxy data of summer rainfall over eastern China, *Geophys. Res. Lett.*, 33, doi:10.1029/2005GL024804.

Smith, T. M., R. W. Reynolds, T. C. Peterson, and J. Lawrimore (2008), Improvements to NOAA's historical merged land-ocean surface temperature analysis (1880–2006), *J. Clim.*, *21*, 2283–2296, doi:10.1175/2007JCLI2100.1.

Sultan, B., and S. Janicot (2003), The West African monsoon dynamics. Part II: The "preonset'" and "onset" of the summer monsoon, *J. Clim.*, 16, 3407–3427.

Taylor, K. E., R. J. Stouffer, and G. A. Meehl (2012), An overview of CMIP5 and the experiment design, *Bull. Amer. Meteor. Soc.*, 93, 485–498.

Ting, M., Y. Kushnir, R. Seager, and C. Li (2009), Forced and internal 20th century SST trends in the North Atlantic, *J. Clim.*, 22, 1469–1481.

Ting, M., Y. Kushnir, R. Seager, and C. Li (2011), Robust features of Atlantic multi-decadal variability and its climate impacts, *Geophys. Res. Lett.*, 38(17), doi:10.1029/2011GL048712.

Ting, M., Y. Kushnir, R. Seager, and C. Li (2014), North Atlantic Multidecadal SST Oscillation: External forcing versus internal variability, *J. Mar. Sys.*, 133, 27–38.

Tourre, Y. M., B. Rajagopalan, Y. Kushnir, M. Barlow, and W. B. White (2001), Patterns of coherent decadal and interdecadal climate signals in the Pacific Basin during the 20th century, Geophys. Res.

492 Lett., 28(10), 2069–2072.
493
494 Trenberth, K. E., and J. W. Hurrell (1994), Decadal atmosphere-ocean variations in the Pacific,
495 *Clim. Dyn.*, 9, 303–319.
496
497 Vizy, E. K., K. H. Cook, J. Crétat, and N. Neupane (2013) Projections of a Wetter Sahel in the
498 Twenty-First Century from Global and Regional Models, *J. Clim.*, 26(13), 4664–4687.
499
500 Wang, X., A. S. Auler, R. L. Edwards, H. Cheng, E. Ito, Y. Wang, X. Kong, and M. Solheid (2007),
501 Millennial-scale precipitation changes in southern Brazil over the past 90,000 years, *Geophys. Res.*
502 *Lett*., 34(23).
503
504 Zeng, N., J. D. Neelin, K. M. Lau, and C. J. Tucker (1999), Enhancement of interdecadal climate
505 variability in the Sahel by vegetation interaction, *Science*, 286, 1537–1540.
506
507 Zhang, Y., J. M. Wallace, and D. S. Battisti (1997), ENSO-like interdecadal variability: 1900-93, *J.*
508 *Clim.*, 10(5), 1004-1020.
509
510 Zhang, R., and T. L. Delworth (2006), Impact of Atlantic multidecadal oscillations on India/Sahel
511 rainfall and Atlantic hurricanes, *Geophys. Res. Lett*., 33, doi:10.1029/2006GL026267.
512
513 **Figure captions:**
514

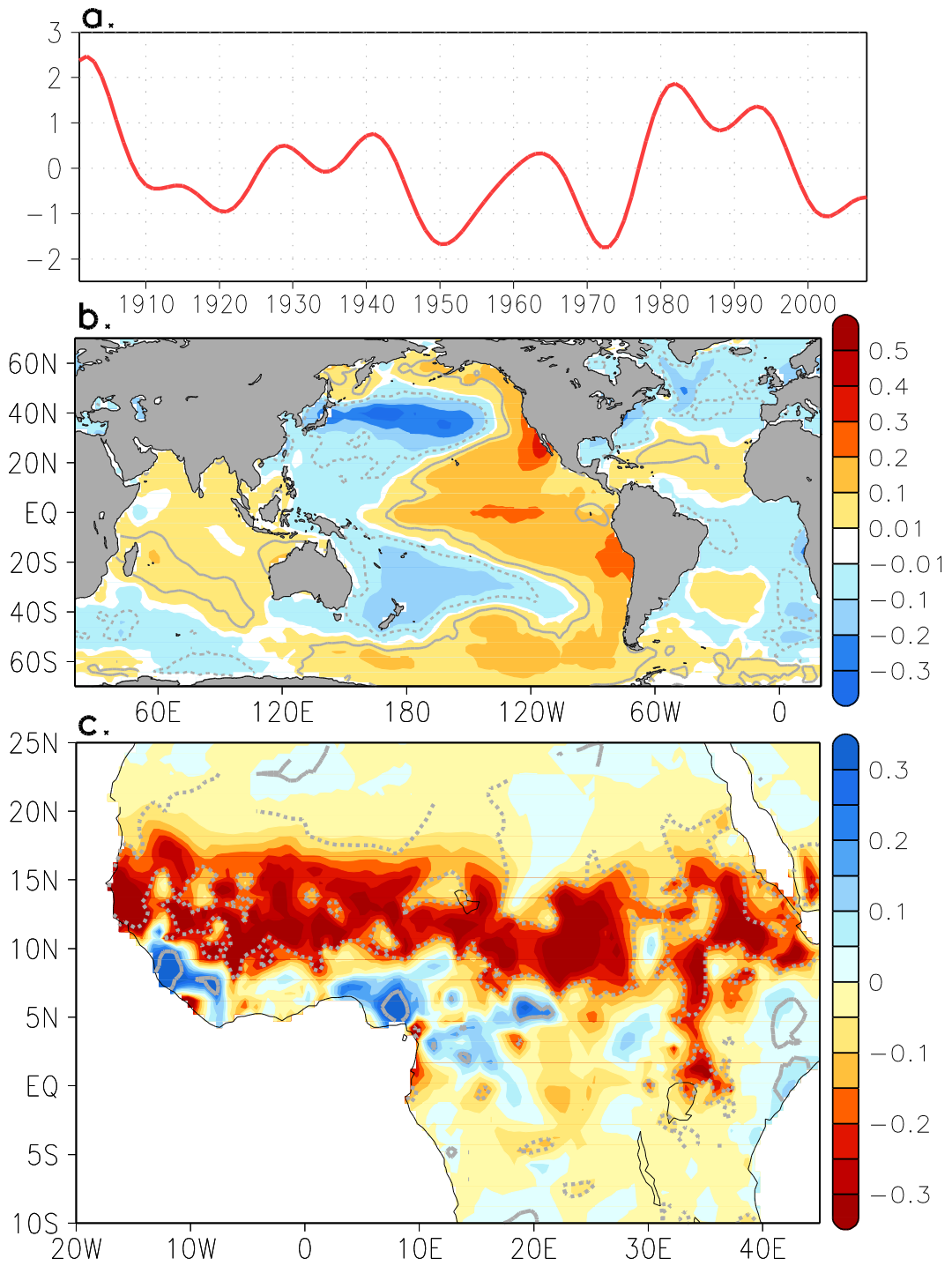

Figure 1. (a) Standardized IPO index obtained with ERSSTv3 from 1901-2008 as defined in the text. **(b)** IPO SST pattern defined as the regression of the unfiltered ERSSTv3 SSTA onto the standardized IPO index (units are K per standard deviation). **(c)** Regression map of unfiltered CRUTS2.1 JAS precipitation anomaly onto the standardized IPO index (units are mm/day per standard deviation). Grey contours in **(b)** and **(c)** indicate the regions where the correlation is significant with a significance level of 0.05 (from a t-test).

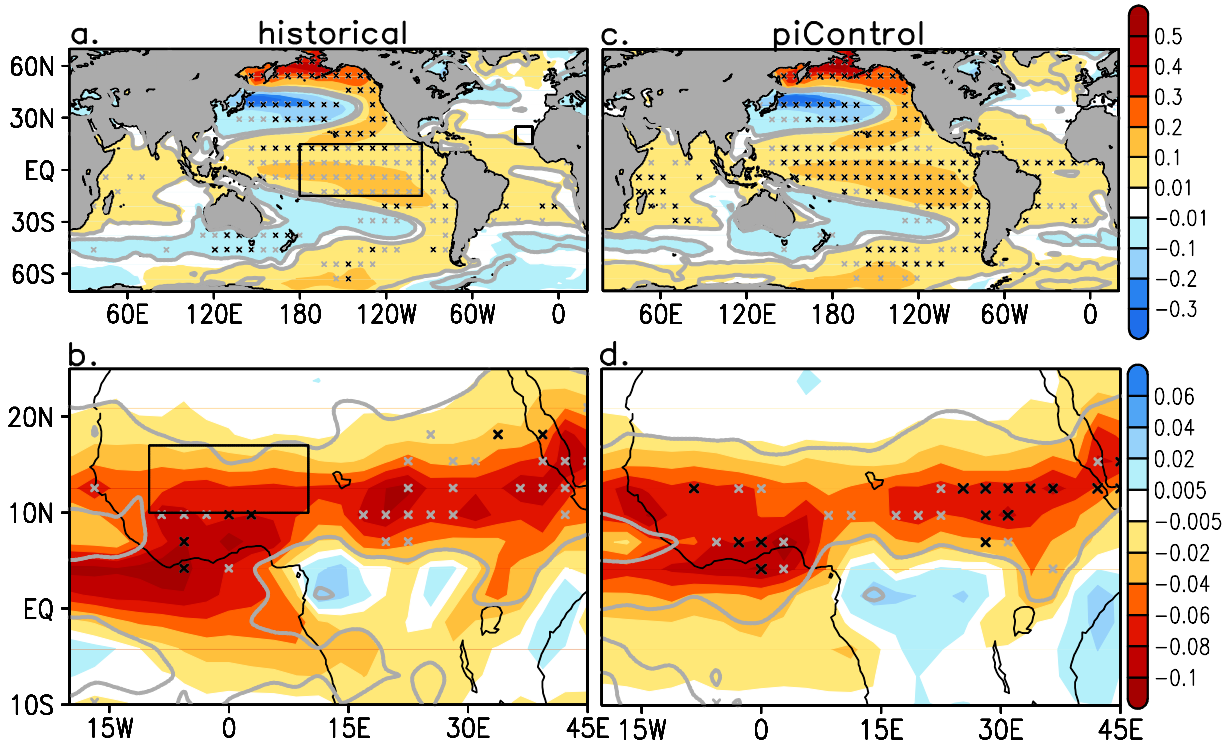

Figure 2. Regression onto the IPO index of the unfiltered **(a)** SSTA (K per std. dev.) and **(b)** JAS precipitation anomalies (mm/day per std. dev.) averaged over the 17 CMIP5 models in the historical run, typically from 1850-2005 (details in Table S1). **(c)** and **(d)** same as **(a)** and **(b)** but for the piControl run. Black and grey marks indicate points where the regression coefficient sign coincides in at least 13 and 15 out of the 17 models analyzed, respectively. Grey contours indicate the regions where the averaged correlation is significant at alpha=0.05 (using a Monte Carlo-based test, see details in the supplementary material).

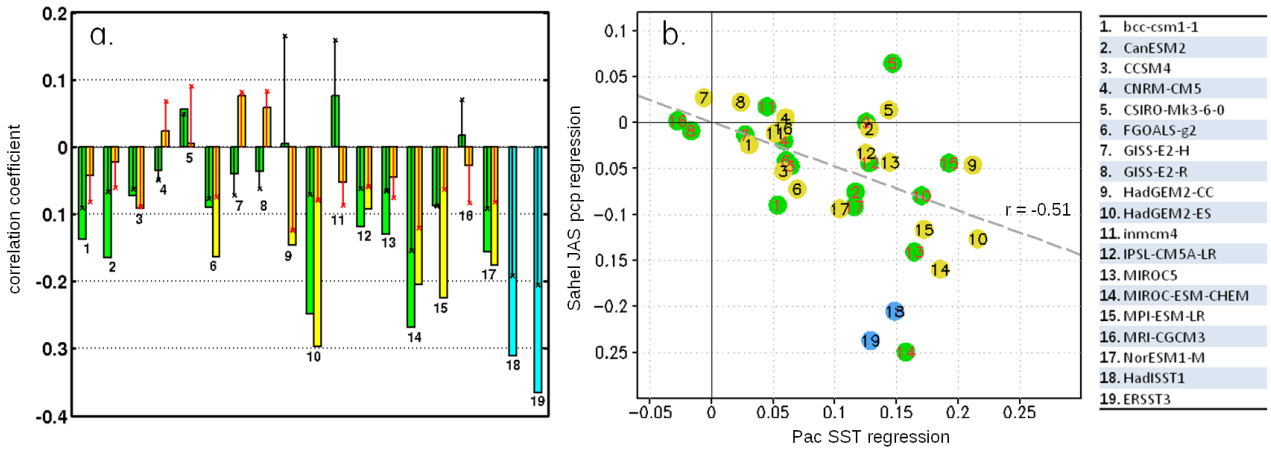

533

534 **Figure 3. (a)** Bar chart of correlation coefficient between IPO index and the unfiltered time series
535 of the precipitation anomaly averaged over Sahel (between 17º-10ºN and 10ºW-10ºE, see box in
536 Figure 2b) for the ensemble-mean historical simulations and observations (green) and piControl
537 runs (yellow). The stems indicate the correlation threshold for statistical significance at alpha=0.05
538 (using a Monte Carlo-based test, see details in the supplementary material). (**b)** Scatter plot of the
539 regression coefficient of precipitation anomaly over Sahel (between 17º-10ºN and 10ºW-10ºE, see
540 box in Figure 2b) (units are mm/day per std. dev.), and the Tropical Pacific (15ºN-15ºS and 180º-
541 95ºW, see box over the Pacific in Figure 2a) SSTA (units are K per std. dev.). The regression line
542 fitted to all the points has a correlation coefficient R=-0.51. Numbers from 1 to 17 correspond to
543 single models; 18 and 19 correspond to observations.

544

545

546

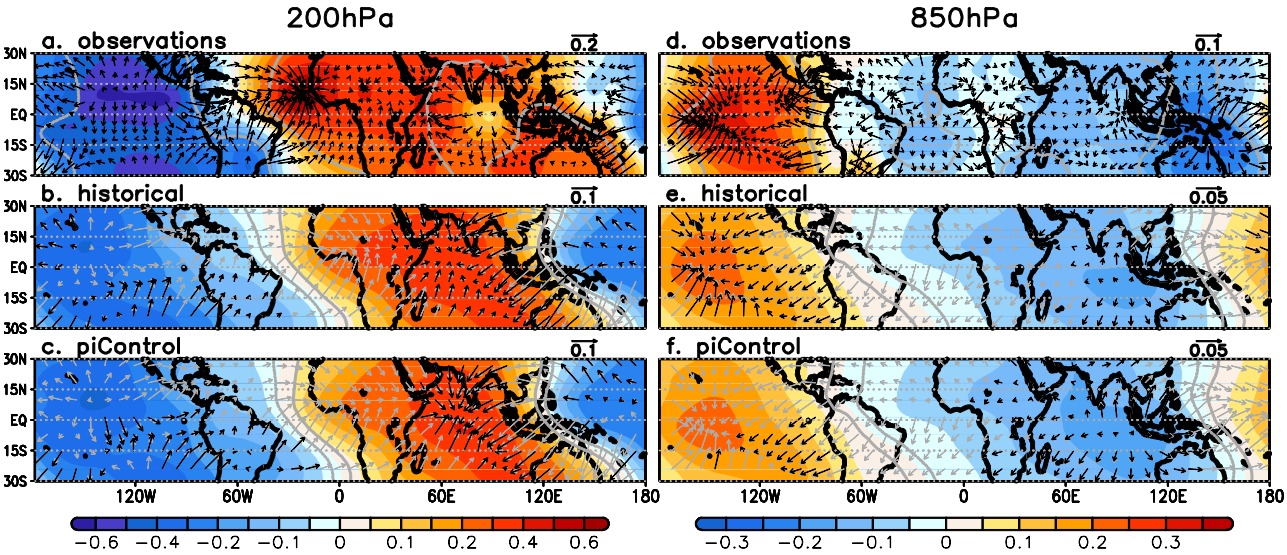

547

548 **Figure 4. (a)** Regression of the unfiltered JAS anomaly of velocity potential at 200 hPa from 20th
549 Century Reanalysis (1901-2008) onto the IPO index; **(b)** and **(c)** same as **(a)** but for the averaged
550 regression in the historical and piControl simulations, respectively; **(d)**, **(e)** and **(f)** same as **(a)**, **(b)**
551 and **(c)** but for the velocity potential at 850 hPa (10^6 m^2/s per std. dev.). Vectors represent the
552 divergent wind; in black at points where the sign of the regression coefficient of the velocity
553 potential coincides in at least 15 out of the 17 models analyzed and in grey at the rest of the points
554 in **(b)**, **(c)**, **(e)** and **(f)**. Grey contours indicate the regions where the averaged correlation is
555 significant at alpha=0.05 (using a Monte Carlo-based test, see details in the supplementary
556 material).

557

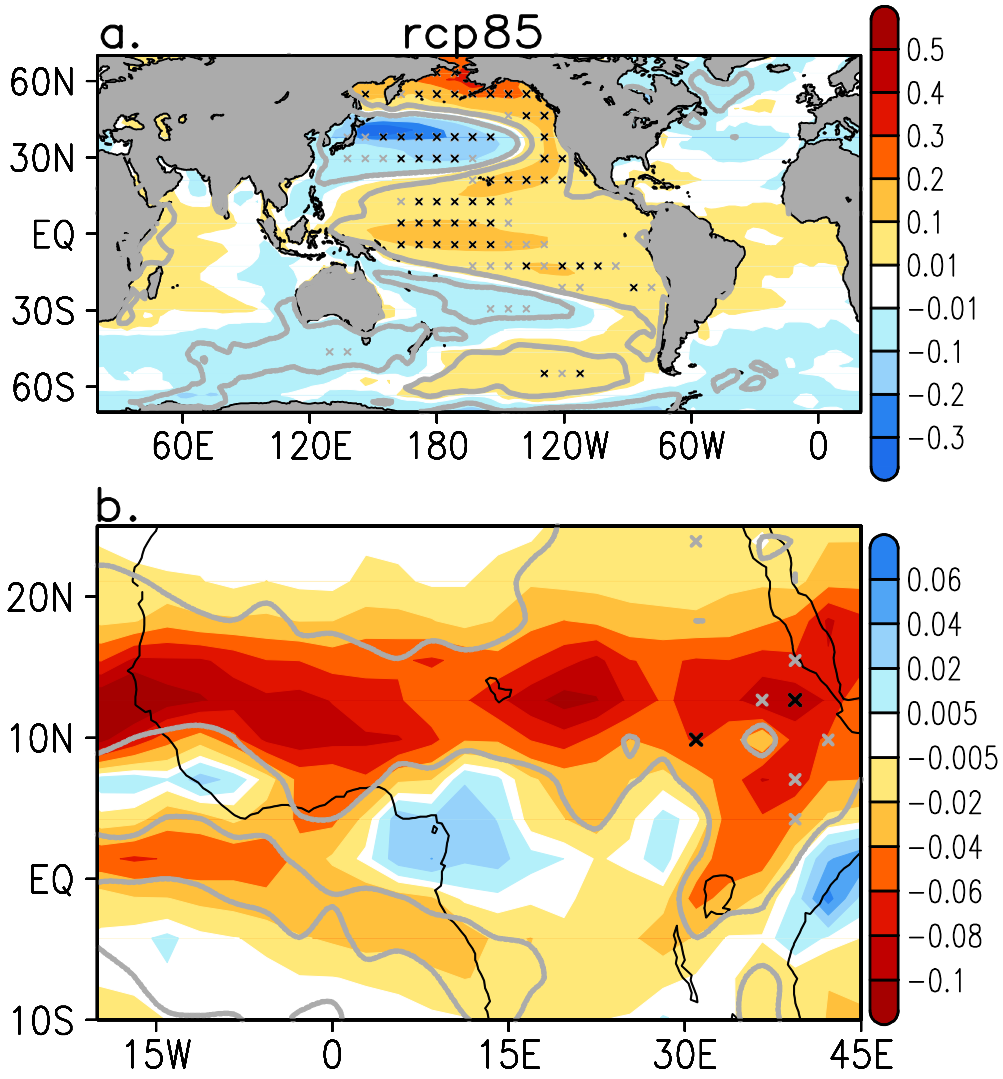

558

559 **Figure 5.** Regression onto the IPO index of the unfiltered **(a)** SSTA (K per std. dev.) and **(b)** JAS
560 precipitation anomalies (mm/day per std. dev.) averaged over the 17 CMIP5 models in the rcp8.5
561 run, typically from 2006-2100 (details in Table S1). Black and grey marks indicate points where
562 the regression coefficient sign coincides in at least 13 and 15 out of the 17 models analyzed,
563 respectively. Grey contours indicate the regions where the averaged correlation is significant at
564 alpha=0.05 (using a Monte Carlo-based test, see details in the supplementary material).

565